**Tenth International Conference on Computational Fluid Dynamics (ICCFD10), Barcelona,Spain, July 9-13, 2018**

**ICCFD10-2018-111**

# A Monolithic Fluid-Structure Algorithm Applied to Buckling of Red Blood Cell Membrane

A. Cetin* and M. Sahin*
Corresponding author: cetinay@itu.edu.tr

*Faculty of Aeronautics and Astronautics Engineering, Istanbul Technical University Maslak, Istanbul, 34469, TURKEY.

**Abstract:** A parallel monolithic fluid-structure interaction (FSI) algorithm presented in [Eken and Sahin, A parallel monolithic algorithm for the numerical simulation of large scale fluid structure interaction problems. International Journal for Numerical Methods in Fluids, 80:687-714, (2016)] has been used to investigate the deformation of red blood cells (RBCs) in small capillaries, where cell deformability has significant effects on blood rheology. The method employs the divergence-free side-centered unstructured finite volume method based on Arbitrary Lagrangian-Eulerian (ALE) formulation for the fluid domain and the classical Galerkin finite element formulation for the Saint Venant-Kirchhoff material in a Lagrangian frame for the solid domain. The compatible kinematic boundary condition is utilized at the fluid-solid interface in order to conserve the mass of cytoplasmic fluid within the red cell membrane at machine precision. The resulting large scale algebraic equations are solved in a fully coupled manner using a new matrix factorization similar to that of the projection method and the parallel algebraic multigrid solver BoomerAMG provided by the HYPRE library is used for the blocks corresponding to the scaled discrete Laplacian and the diagonal blocks of the elasticity equation. The numerical simulations initially indicate a complex shape deformation in which biconcave discoid shape changes to a parachute-like shape and then the parachute-like cell shape undergoes a cupcake shaped buckling instability for a relatively small capillarity diameter ($10\mu m$). The instability forms thin rib-like features and the red cell deformation is not axisymmetric but three-dimensional. The azimuthal wavenumber of the instability is also relatively high and it is computationally challenging to resolve.

*Keywords:* Fluid-Structure Interaction, Red Blood Cell, Monolithic Method, Buckling Instability.

## 1 Introduction

Red blood cells, also called erythrocytes, can be defined as nucleus-free deformable liquid capsules enclosed by a biological membrane that is nearly incompressible and exhibits a viscoelastic response to shearing and bending deformation. The mechanical properties of red cells strongly influence the rheological behavior of blood and introduce non-Newtonian effects. A number of human diseases such as hypertension, malaria, sickle cell anemia and diabetes mellitus leads to change in the mechanical properties of red blood cells and reduction in deformability, which increase in microvascular flow resistance and a decrease in cellular oxygen delivery.

The numerical studies to determine the red cell behaviors in various flow situations have been based on lubrication theory [1], boundary integral method [2], immersed boundary method [3], lattice Boltzmann method [4], etc. In contrast to the above studies, there are very limited works on the fluid-structure interaction (FSI) of red blood cells based on body conformal meshes with a finite membrane thickness. To the best of our knowledge, only Klöppel and Wall [5] employed the fluid-structure interaction (FSI) algorithm with finite thickness solid shell elements in three-dimensions for the red cell membrane and investigated the mechanical behavior of human red blood cell filled with a Newtonian fluid in optical tweezers. The reason is that

the classical partitioned (segregated) approaches can not satisfy the incompressibility constraint of the fluid during standard alternating FSI iterations when the fluid domain is entirely enclosed by all Dirichlet boundary conditions as pointed out by [6]. There is also problem with the high aspect ratio of solid shell elements employed within relatively thin lipid bilayer ($5nm$). In the present approach, the fluid domain is discretized using the stable side-centered unstructured finite volume method based on Arbitrary Lagrangian-Eulerian (ALE) formulation, meanwhile the solid domain is discretized with the classical Galerkin finite element formulation for the Saint Venant-Kirchhoff material in a Lagrangian frame [7, 8]. The method employs conformal hexahedral elements at the fluid-solid interface in order to accurately resolve sharp gradients. In addition, the local and global geometric conservation laws (DGCL) [9] are satisfied at discrete level and the compatible kinematic boundary condition is applied at the fluid-solid interface [8] in order to conserve the cytoplasmic fluid mass at machine precision. In the current paper, the resulting large-scale algebraic linear systems are solved in a fully coupled (monolithic) manner using the FGMRES($m$) Krylov iterative method [10] preconditioned with a matrix factorization similar to that of the projection method [11] for the whole system and the parallel algebraic multigrid solver BoomerAMG provided by the HYPRE library [12], which we access through the PETSc library [13], is used for the scaled discrete Laplacian and and diagonal blocks of the elasticity equation. The present new block preconditioner may be considered as the extension of the classical projection method [11] to FSI problems. The numerical calculations reveal that the biconcave discoid shape initially changes to a parachute-like shape and then the parachute shaped red cell membrane undergoes a cupcake shaped buckling instability for a relatively small capillarity diameter, which has not been observed in the literature. The instability forms thin rib-like features and the red cell deformation is not axisymmetric but three-dimensional. The azimuthal wavenumber of the instability is also relatively high and it is computationally challenging to resolve.

# 2 Problem Statement

## 2.1 Fluid Equations

The integral form of incompressible Navier-Stokes equations can be written in the Cartesian coordinate system in dimensional form. The momentum and the continuity equations can be written as;

$$\rho_f \frac{\partial}{\partial t} \int_\Omega \mathbf{u} \mathrm{d}V + \rho_f \oint_{\partial\Omega} [\mathbf{n} \cdot (\mathbf{u} - \dot{\mathbf{x}})] \mathbf{u} \mathrm{d}S = \oint_{\partial\Omega} \sigma_f \mathbf{n} \mathrm{d}S \tag{1}$$

$$- \oint_{\partial\Omega} \mathbf{n} \cdot \mathbf{u} \mathrm{d}S = 0 \tag{2}$$

In these equations $V$ is control volume, $S$ is the control volume surface area, $\mathbf{n}$ is the outward normal vector, $\rho_f$ is the fluid constant density, $\mathbf{u}$ is the local fluid velocity vector, $\dot{\mathbf{x}}$ is the grid velocity and $\sigma_f$ is the fluid stress tensor. The constitutive relation for the fluid stress tensor is given for an incompressible Newtonian fluid by

$$\sigma_f = -p\mathbf{I} + \mu_f(\nabla \mathbf{u} + \nabla \mathbf{u}^\top) \tag{3}$$

where $p$ is the fluid pressure and $\mu_f$ is the fluid dynamic viscosity.

## 2.2 Solid Equation

Balance of linear momentum in the Lagrangian framework where the material derivative becomes a partial derivative with respect to time governs the structural behavior.

$$\rho_s \frac{\partial^2 \mathbf{d}}{\partial t^2} = \nabla \sigma_s \tag{4}$$

where $\rho_s$ is the the spatial density, $\mathbf{d}$ is the displacement vector, $\sigma_s$ is the Cauchy stress tensor defined using the following constitutive law for the St. Venant-Kirchhoff material:

$$S = J\mathbf{F}^{-1} \sigma_s \mathbf{F}^{-\top} \tag{5}$$

$$\mathbf{F} = (\mathbf{I} + \nabla \mathbf{d}) \tag{6}$$

$$E = \frac{1}{2}(\mathbf{F}^\top \mathbf{F} - \mathbf{I}) \tag{7}$$

$$S = \lambda_s trace(\mathbf{E})\mathbf{I} + 2\mu_s \mathbf{E} \tag{8}$$

$$\Pi = \mathbf{F}\mathbf{S} \tag{9}$$

where $\mathbf{S}$ is the second Piola-Kirchhoff stress tensor, $\mathbf{F}$ is the deformation gradient tensor, $J = det(\mathbf{F})$ is the deformation gradient determinant, $\mathbf{E}$ is the Green-Lagrange strain tensor, $\Pi$ is the non-symmetric first Piola-Kirchhoff stress tensor and $\lambda_s$ and $\mu_s$ are the material Lame's constants. Then the initial equation can be written as

$$\rho_0 \frac{\partial^2 \mathbf{d}}{\partial t^2} = \nabla_0 \cdot \Pi^\top \tag{10}$$

where $\rho_0$ is the solid material density per unit undeformed volume and $\nabla_0$ states the gradient in Lagrangian coordinates.

### 2.3 Interface Condition Equations

Interface condition requires two main conditions, which are the kinematic and the dynamic continuity across the fluid-structure interface at all times. The kinematic boundary condition on the fluid-structure interface is driven by continuity of the velocity.

$$\mathbf{u} = \dot{\mathbf{d}} \tag{11}$$

where $\mathbf{u}$ is local fluid velocity vector and $\dot{\mathbf{d}}$ is time derivative of structure displacement vector. The dynamic condition holds for surface traction at the common fluid-structure interaction boundary.

$$\sigma_s \mathbf{n}_s = -\sigma_f \mathbf{n}_f \tag{12}$$

where $\sigma_s$ is the Cauchy stress tensor of the solid and $\sigma_f$ is the stress tensor in the case of an incompressible Newtonian fluid.

## 3 Numerical Results

The outer surface geometry of the red blood cell is defined with the following equation [14, 15] and the geometry of red blood cell is given in Figure 1.

$$T(r) = \pm\sqrt{1-(r/R_0)^2}\left[C_0 + C_1(r/R_0)^2 + C_2(r/R_0)^4\right] \tag{13}$$

In here, $T(r)$ is the thickness of RBC in the $x-$direction as a function of the distance $r = \sqrt{y^2+z^2}$ and $R_0$ is the initial radius of RBC. The geometric parameters are taken to be $R_0 = 3.9\mu m$, $C_0 = 0.81\mu m$, $C_1 = 7.83\mu m$ and $C_2 = -4.39\mu m$. The minimum thickness is $T_1 = 0.81\mu m$ and the maximum thickness is $T_2 = 2.4\mu m$. The diameter of the red blood cell is $D = 7.8\mu m$. The thickness of the red cell membrane is approximately $40 - 50nm$ [16, 17] and the internal surface of the red blood cell is formed with an inward thickness of $h = 0.05m$ $(50nm)$. The physical parameters of the red blood cell and fluid plasma are tabulated in Table 1. The calculations are carried out on three different meshes: coarse mesh M1, medium mesh M2,

Table 1: Physical parameters for red blood cell ($pg$ : picogram).

| | | | |
|---|---|---|---|
| Fluid | Density, $\rho_f$ | $[pg/\mu m^3]$ | 1.025 |
| | Dynamic Viscosity, $\mu_f$ | $[pg/\mu m\mu s]$ | 1.1 |
| | Maximum inflow velocity, $U_{max}$ | $[\mu m/\mu s]$ | 0.01 |
| Structure | Density, $\rho_s$ | $[pg/\mu m^3]$ | 1.098 |
| | Poison Ratio, $\nu_s$ | $-$ | 0.45 |
| | Elasticity Module, $E$ | $[pg/\mu m\mu s^2]$ | 4.4 |

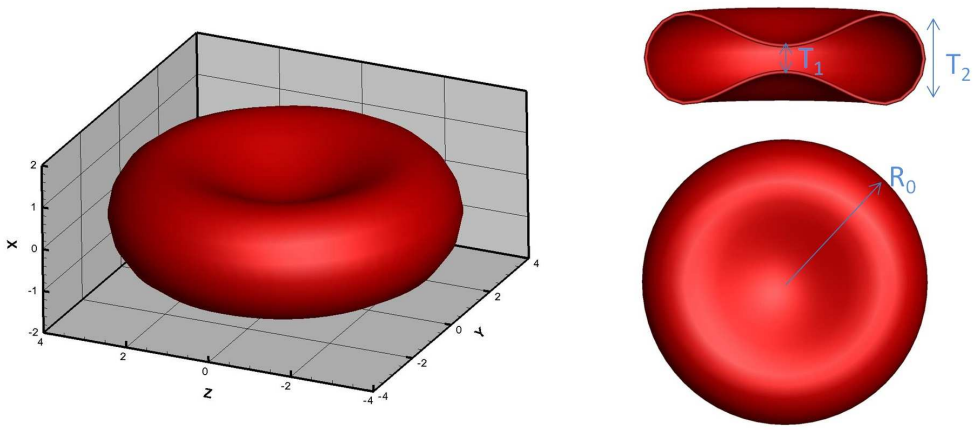


Figure 1: Geometry of red blood cell.

and fine mesh M3. The successive meshes are generated with DISTENE MeshGems-Hexa algorithm in three-dimensions based on the octree method by halving the mesh size function. The details of the computational meshes are provided in Table 2. The number of solid layers indicates the number of quadrilateral elements in the normal direction for the solid membrane. The maximum aspect ratio of solid quadrilateral elements is set to 20. $\Delta h_{min}$ and $\Delta h_{max}$ represent the minimum and maximum mesh sizes, respectively. The capillary tube spans between $\pm 70\mu m$, where the red cell is initially located at the origin. The boundary conditions are set to no-slip boundary conditions on the solid walls, the Dirichlet (parabolic profile) velocity at the inlet and the natural (traction-free) boundary condition at the outlet. The maximum velocity for the paraboloid inlet profile is set to $0.01\mu m/\mu s$. The calculations are started from the rest and the time step is set to $100\mu s$. In the present numerical simulation, it is rather difficult to resolve the relatively thin lipid bilayer ($5nm$), which mainly contributes the membrane shear modulus. Therefore the elasticity module in Table 1 is reduced by a factor of 10 in order to achieve the same overall membrane shear module ($\mu_s h = 7.586 \times 10^{-6} N/m$). The non-dimensional capillary number ($Ca = \mu_f U_{max}/\mu_s h$) is obtained to be 0.145 based on the shear modulus $\mu_s$, the maximum inlet velocity $U_{max}$, the plasma dynamic viscosity $\mu_f$, and the membrane thickness $h$. The computed contours of $u-$velocity component on $z = 0$ plane and the velocity profile around the red cell are provided in Figure 2-a at $t = 60ms$. The blunt velocity profile around the red cell is clearly apparent. The three-dimensional views of the time variations of the red cell deformation and its movement at several different time levels are provided in Figure 2-b. The numerical simulations indicate a complex shape deformation in which the biconcave discoid shape changes to a parachute-like shape and then then parachute-like shape undergoes a cupcake shaped buckling instability in three-dimensions due to the compressive elastic tension forces along the red cell membrane surface. To the best of our knowledge, the present cupcake shaped buckling instability in small capillary tubes has not been noticed in three-dimensional simulations in the literature (see, for example, [18, 19]). One possibility may be the lack of sufficient initial random disturbances, which leads to a buckling instability due to the amplification of these random disturbances. This is particularly important for spectral type approaches as in [19]. The second possibility is that [20] law applied to the spherical capsule buckling produces a wider stability interval than the neo-Hooken law due to its strain hardening nature [21]. The present Saint Venant-Kirchhoff constitutive law does not show strain hardening property in the case of the compression of a body to zero volume, where the stress approaches zero instead of infinity. The third possibility is that the present bending stiffness value is relatively lower compared

Table 2: Computational meshes used for simulation of red blood cell for a channel height of $10.0\mu m$.

| Mesh | Solid layers | $\Delta h_{min}$ | $\Delta h_{max}$ | Node number | Element number | DOF |
|---|---|---|---|---|---|---|
| M1 | 4 | 0.25 | 1 | 61,592 | 57,233 | 668,461 |
| M2 | 8 | 0.125 | 0.5 | 419,216 | 402,391 | 4,406,485 |
| M3 | 16 | 0.0625 | 0.25 | 2,836,912 | 2,786,273 | 29,090,781 |

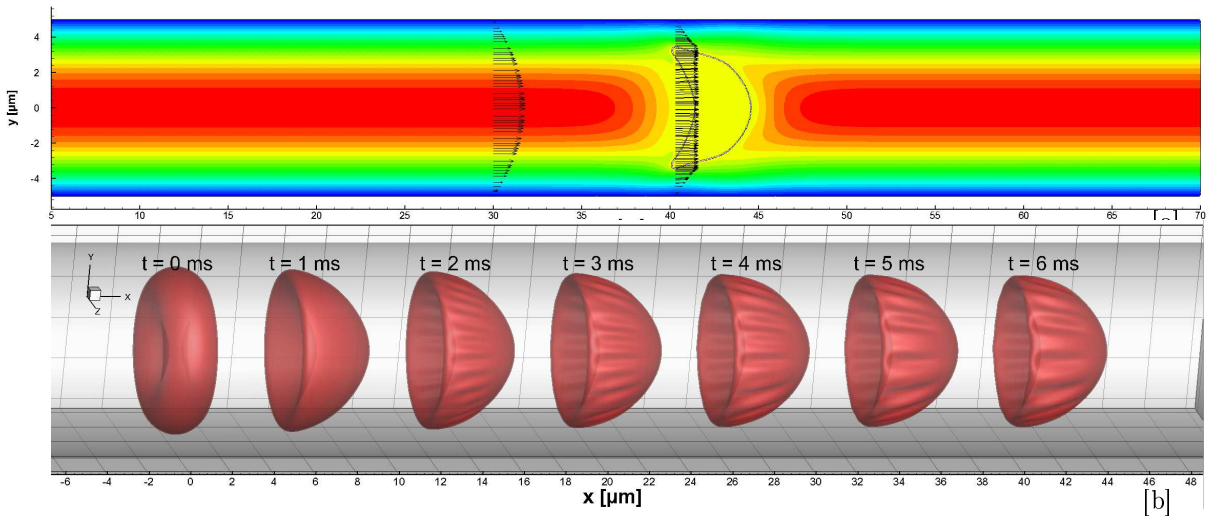


Figure 2: Red blood cell positions/deformations with computed $u-$velocity component contours on $z = 0$ plane at $t = 60ms$ [a] and red cell deformations at several different time levels for a single red blood cell for a capillary tube diameter of $10\mu m$ on mesh M3.

to the values used in the classical membrane models. Another possibility is that the wavenumber in the azimuthal direction may increase significantly with the decrease in the membrane thickness and the required mesh resolution may be underestimated in this direction [22]. The spatial convergence of the cupcake shaped membrane buckling instability is provided in Figure 3 for a capillary tube diameter of $10\mu m$ on meshes M1 to M3. The simulation on mesh M3 leads to a relatively large FSI simulation with 29,090,781 DOF. The buckling instability forms thin rib-like features and the deformation is not axisymmetric but three-dimensional. The spherical fluid-filled capsule deformed in axisymmetric elongational flow also indicates the similar buckling instability [21]. However, the buckling on the red cell membrane leads to relatively more complex instability due to its initial biconcave discoid shape compared to that of the oblate spheroidal capsule [23]. The present wavenumber of the buckling instability is even higher during the initial formation of the buckling with more uniform distribution and the rib-like features tend to merge with the increased deformation, forming larger structures as seen in Figure 4. Therefore, the post-buckling behavior of the red cell membrane is highly unstable and non-linear, which is in accord with the observations related to the spherical capsules [22].

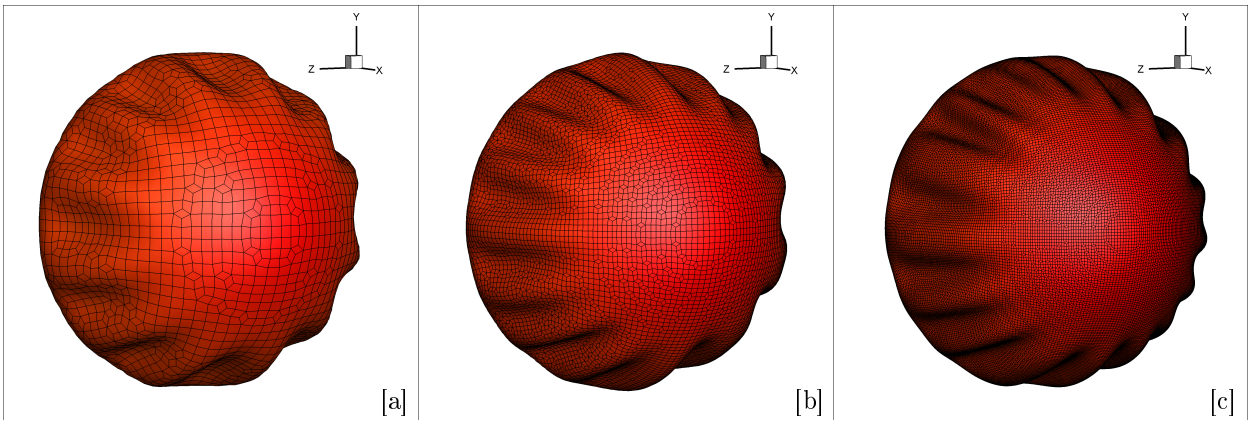


Figure 3: Mesh convergence of cupcake shaped membrane buckling instability on mesh M1 [a], mesh M2 [b] and mesh M3 [c] for a capillary tube diameter of $10\mu m$ at $t = 60ms$.

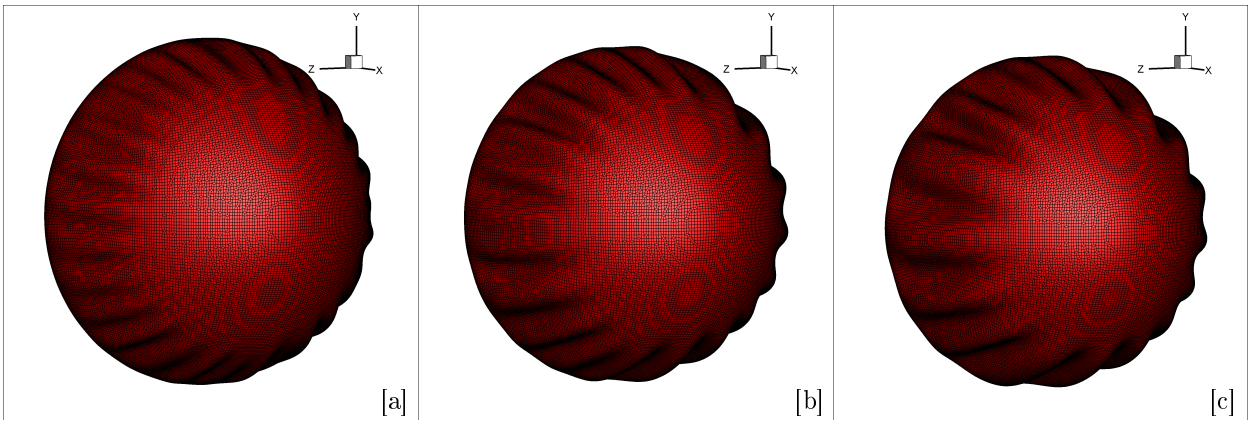


Figure 4: Time evolution of cupcake shaped membrane buckling instability on mesh M3 at $t = 20ms$ [a], $t = 40ms$ [b] and $t = 60ms$ [c] for a capillary tube diameter of $10\mu m$.

# 4 Conclusion

The parallel fully coupled (monolithic) fluid-structure interaction approach [7, 8] has been applied to investigate the deformation of red blood cells in small capillaries. A special attention is given to conserve the mass of the cytoplasmic fluid within the red cell. The calculations show a complex shape deformation in which the biconcave discoid shape changes to a parachute-like shape, which is in accord with the early results in the literature. In addition, the red cells in small capillaries undergo a cupcake shaped buckling instability forming thin rib-like features in three-dimensions due to the compressive elastic tension forces along the membrane surface and the resulting red cell geometry is no longer axisymmetric but three-dimensional. The wavenumber of the instability in the azimuthal direction is also relatively high and it is computationally challenging to resolve. To our best knowledge, the cupcake shaped buckling instability in small capillaries has not been noted in the literature. Although the simplest type of hyperelastic material model is used in the current simulations, the present buckling instability should be confirmed using more realistic solid red cell membrane models as in the work of [5].

# References

[1] T. W. Secomb. Flow-dependent rheological oroperties of blood in capillaries. *Microvascular Research*, 34:46–58, 1987.

[2] C Pozrikidis. Axisymmetric motion of a file of red blood cells through capillaries. *Physics of Fluids*, 17(3):031503, 2005.

[3] Charles D Eggleton and Aleksander S Popel. Large deformation of red blood cell ghosts in a simple shear flow. *Physics of Fluids*, 10(8):1834–1845, 1998.

[4] Daniel A. Reasor Jr, Jonathan R. Clausen, and Cyrus K. Aidun. Coupling the lattice-Boltzmann and spectrin-link methods for the direct numerical simulation of cellular blood flow. *International Journal for Numerical Methods in Fluids*, 68:767–781, 2012.

[5] Thomas Klöppel and Wolfgang A Wall. A novel two-layer, coupled finite element approach for modeling the nonlinear elastic and viscoelastic behavior of human erythrocytes. *Biomechanics and Modeling in Mechanobiology*, 10(4):445–459, 2011.

[6] Ulrich Küttler, Christiane Förster, and Wolfgang A Wall. A solution for the incompressibility dilemma in partitioned fluid-structure interaction with pure Dirichlet fluid domains. *Computational Mechanics*, 38(4):417–429, 2006.

[7] Ali Eken and Mehmet Sahin. A parallel monolithic algorithm for the numerical simulation of large-scale fluid structure interaction problems. *International Journal for Numerical Methods in Fluids*, 80(12):687–714, 2016.

[8] Ali Eken and Mehmet Sahin. A parallel monolithic approach for fluid-structure interaction in a cerebral aneurysm. *Computers and Fluids*, 153:61–75, 2017.

[9] P. D. Thomas and C. K. Lombard. Geometric conservation law and its application to flow computations on moving grids. *AIAA Journal*, 17:1030–1037, October 1979.

[10] Youcef Saad. A flexible inner-outer preconditioned GMRES algorithm. *SIAM Journal on Scientific Computing*, 14(2):461–469, march 1993.

[11] Alexandre Joel Chorin. Numerical solution of the Navier-Stokes equations. *Mathematics of Computation*, 22(104):745–762, 1968.

[12] R. Falgout, A. Baker, E. Chow, V.E Henson, E. Hill, J. Jones, T. Kolev, B. Lee, J. Painter, C. Tong, P. Vassilevski, and U. M. Yang. *Users manual, HYPRE High Performance Preconditioners, UCRL-MA-137155 DR*. Center for Applied Scientific Computing, Lawrence Livermore National Laboratory, 2004.

[13] Satish Balay, Shrirang Abhyankar, Mark F. Adams, Jed Brown, Peter Brune, Kris Buschelman, Lisandro Dalcin, Victor Eijkhout, William D. Gropp, Dinesh Kaushik, Matthew G. Knepley, Lois Curfman McInnes, Karl Rupp, Barry F. Smith, Stefano Zampini, Hong Zhang, and Hong Zhang. PETSc users manual. Technical Report ANL-95/11 - Revision 3.8, Argonne National Laboratory, 2017.

[14] Evan Evans and Yuan-Cheng Fung. Improved measurements of the erythrocyte geometry. *Microvascular Research*, 4(4):335–347, 1972.

[15] Tenghu Wu and James J Feng. Simulation of malaria-infected red blood cells in microfluidic channels: Passage and blockage. *Biomicrofluidics*, 7(4):044115, 2013.

[16] Volkmar Heinrich, Ken Ritchie, Narla Mohandas, , and Evan Evans. Elastic thickness compressibilty of the red cell membrane. *Biophysical Journal*, 81:1452–1463, 2001.

[17] Young-Zoon Yoon, Jurij Kotar, Gilwon Yoon, and Pietro Cicuta. The nonlinear mechanical response of the red blood cell. *Physical Biology*, 5:036007, 2008.

[18] Xing Shi, Guang Lin, Jianfeng Zou, and Dmitry A Fedosov. A lattice Boltzmann fictitious domain method for modeling red blood cell deformation and multiple-cell hydrodynamic interactions in flow. *International Journal for Numerical Methods in Fluids*, 72(8):895–911, 2013.

[19] Hong Zhao, Amir HG Isfahani, Luke N Olson, and Jonathan B Freund. A spectral boundary integral method for flowing blood cells. *Journal of Computational Physics*, 229(10):3726–3744, 2010.

[20] R Skalak, A Tozeren, RP Zarda, and S Chien. Strain energy function of red blood cell membranes. *Biophysical Journal*, 13(3):245–264, 1973.

[21] E. Lac, D. Barthes-Biesel, N. A. Pelekasis, and J. Tsamopoulos. Spherical capsules in three-dimensional unbounded Stokes flows: Effect of the membrane constitutive law and onset of buckling. *Journal of Fluid Mechanics*, 516:303–334, 2004.

[22] X.-Q. Hu, A.-V. Salsac, and D. Barthés-Biesel. Flow of a spherical capsule in a pore with circular or square cross-section. *Journal of Fluid Mechanics*, 2012:176–194, 2012.

[23] Wei-Xi Huang, Cheong Bong Chang, and Hyung Jin Sung. Three-dimensional simulation of elastic capsules in shear flow by the penalty immersed boundary method. *Journal of Computational Physics*, 231(8):3340–3364, 2012.